# High-power single-mode vertical-cavity surface-emitting lasers using strain-controlled disorder-defined apertures ©

Cite as: Appl. Phys. Lett. **119**, 241101 (2021); https://doi.org/10.1063/5.0068713 Submitted: 26 August 2021 • Accepted: 25 November 2021 • Published Online: 13 December 2021

🗓 Patrick Su, Kevin P. Pikul, Mark D. Kraman, et al.

#### COLLECTIONS

æ

This paper was selected as an Editor's Pick







# ARTICLES YOU MAY BE INTERESTED IN

High-efficiency circularly polarized green light emission from GaN-based laser diodes integrated with GaN metasurface quarterwave plate

Applied Physics Letters 119, 241103 (2021); https://doi.org/10.1063/5.0067396

Tailoring the spectral properties of layered chiral mid-infrared metamaterials Applied Physics Letters 119, 241102 (2021); https://doi.org/10.1063/5.0066386

A perspective of twisted photonic structures

Applied Physics Letters 119, 240501 (2021); https://doi.org/10.1063/5.0070163





Find out more



# 

Cite as: Appl. Phys. Lett. **119**, 241101 (2021); doi: 10.1063/5.0068713 Submitted: 26 August 2021 · Accepted: 25 November 2021 · Published Online: 13 December 2021







Patrick Su,<sup>a)</sup> (D) Kevin P. Pikul, Mark D. Kraman, and John M. Dallesasse

#### **AFFILIATIONS**

Department of Electrical and Computer Engineering and Holonyak Micro and Nanotechnology Laboratory, University of Illinois at Urbana-Champaign, Urbana, Illinois 61801, USA

<sup>a)</sup>Author to correspondence should be addressed: psu8@illinois.edu

# **ABSTRACT**

Strain-engineered diffusion masks deposited via plasma-enhanced chemical vapor deposition are demonstrated to control the curvature of the zinc diffusion front and, hence, disordering front, in disorder-defined vertical-cavity surface-emitting lasers (VCSELs) for enhanced high-power single-mode operation. Tensilely strained silicon nitride diffusion masks are applied to limit the lateral undercut of the disordering front, thereby minimizing the interaction between the disordered region of the distributed Bragg reflector and the fundamental mode. This results in higher threshold modal gain and absorption losses from the disordered region for higher-order modes while enabling greater output powers for fundamental-mode operation in single-mode impurity-induced disordered VCSEL designs. Using this technique, 850 nm AlGaAs VCSELs are shown to operate in a single fundamental mode with record optical output powers in excess of 10 mW and side-mode suppression ratios greater than 35 dB. Electrical and optical performances of these devices are presented in addition to near-field images confirming single-fundamental-mode lasing.

Published under an exclusive license by AIP Publishing. https://doi.org/10.1063/5.0068713

With the advent of facile recognition in smartphones, verticalcavity surface-emitting lasers (VCSELs) have become ubiquitous. Due to their circular beam shape, high modulation speeds, and energy efficient operation, VCSELs continue to be used in optical transceivers, laser printers, and position sensors in optical computer "mice." Most recently, VCSEL emission characteristics and the ease of forming 2D arrays have enabled applications such as structured light emission for 3D facile recognition and Time-of-Flight (ToF) Light-Detection And Ranging (LiDAR)<sup>1</sup> in consumer handheld devices. This has ushered in a new era of applications referred to as optical 3D sensing. Because of their short cavity length in the growth direction, VCSELs inherently operate in a single longitudinal mode. However, the active device diameter in the transverse direction typically spans several wavelengths, thus leading to lasing in multiple transverse modes. Since the discovery of AlGaAs oxidation by Dallesasse and Holonyak<sup>2,3</sup> and its first application to VCSELs,4 the inclusion of an oxide aperture has become standard for modern VCSEL designs. As the oxide aperture provides not only current confinement but also optical confinement, VCSELs with oxide apertures smaller than about 3  $\mu$ m typically operate in a single fundamental mode. While this is a straight-forward

method of fabricating single-mode VCSELs, these devices have been limited in maximum single-mode power, incapable of surpassing optical output powers greater than a few milliwatts. Moreover, small oxide-aperture VCSELs tend to have worse overall device reliability and shorter mean time to failure as a consequence of the significant self-heating from the narrow oxide aperture. With the emergence of Pulse Amplitude Modulation (PAM) as an important method of sending data at rates beyond 25 gigabits per second, increasing the maximum single-mode power in VCSELs also provides an opportunity to improve the signal-to-noise ratio (SNR) by increasing the separation between power levels.<sup>8,9</sup> Therefore, investigations into methods that enable single-fundamental-mode operation in VCSELs while improving optical output powers have been of great interest. Methods such as surface relief, 10 holey structures, 11 high-contrast gratings, 12 antiguided resonance waveguide structures (ARROW), <sup>13</sup> and anti-phase coatings<sup>14</sup> achieve single-mode lasing by exploiting the spatial discrimination between the fundamental and higher-order modes and selectively raising/lowering optical mirror reflectivity loss 10,12,14 or anti-guiding properties<sup>11,12</sup> of specific optical modes. However, these mode-control techniques have reported single-mode operation with limited output powers between 6 and 7 mW (Refs. 10, 11, and 13) for 5–12  $\mu$ m oxide-aperture devices and require precise etching of the highly conductive cap layer <sup>10–12</sup> or the requirement of regrowth structures, <sup>13</sup> which can become difficult and expensive to scale.

Being recognized by Laidig and Holonyak et al., 15 impurityinduced disordering (IID) selectively modifies the index of refraction, bandgap, optical reflectivity, and conductivity of Al<sub>x</sub>Ga<sub>1-x</sub>As superlattice pairs. 16,17 Since its discovery, IID has been exploited for improved electrical and optical characteristics in high-performance laser diodes designs. 18-24 Through dielectric masking and low-temperature zinc diffusion, the unmasked regions of the top distributed Bragg reflector (DBR) in a VCSEL become selectively intermixed and disordered. Disordering results in lower optical reflectivity<sup>16</sup> and enhanced freecarrier absorption<sup>20</sup> that is effective in suppressing higher-order modes for single-mode operation in IID (also known as Zn-diffused) VCSELs. 19-21,23 In addition, the heavy p-type doping in the diffused region significantly reduces series resistance through the p-DBR,<sup>20</sup> which improves efficiency by reducing Joule heating in IID VCSELs and simultaneously improving high-frequency modulation performance compared to standard designs. 19,22 However, a main limitation in current IID VCSEL designs, particularly for single-mode operation, is the lateral encroachment of the disordering front onto the fundamental mode. This effect greatly reduces optical output power, 18 increases threshold currents, 20 and degrades thermal performance. 18

To mitigate the lateral encroachment of the disordering front, the authors demonstrated the ability to tailor the diffusion front of the disorder-defined aperture using strained silicon nitride (SiNx) diffusion masks deposited via plasma-enhanced chemical vapor deposition (PECVD).<sup>24</sup> Through applying compressive- or tensile-strained films, the vertical or lateral extent of the disordering front is suppressed, respectively. The application of strain to modify interdiffusion rates in superlattices is a known phenomenon in III-V<sup>25</sup> and SiGe/Si<sup>26</sup> superlattices under high-temperature post-growth annealing (700–800 °C). Similar to the use of strain in the diffusion mask,<sup>24</sup> the interdiffusion rates across strained sub-lattice boundaries were also shown to be enhanced/suppressed through the application of biaxial strain.<sup>25-28</sup> However, these reports have only investigated strainenhanced interdiffusion from epitaxially grown lattice-mismatch layers, not from strain originating from the diffusion mask itself. In the work described here, the surface-deposited strained diffusion mask induces strain-enhanced interdiffusion only locally near the top of the DBR where the disordering process occurs. Furthermore, the strained disordering mask is removed after disordering and, therefore, does not impact the electrical or lasing characteristics of the device beyond modifying the shape of the disorder-defined aperture. This work uses the effect of strain-controlled interdiffusion to modify the curvature of the disordering front in IID VCSELs to achieve record high-power single-mode performance.

The epitaxial structure of the VCSELs fabricated in this work first consists of a n-type GaAs substrate, GaAs buffer, 28 pairs of n-type AlAs/Al $_{0.12}$ Ga $_{0.88}$ As (silicon-doped,  $3\times10^{18}$  cm $^{-3}$ ), and four pairs of n-type Al $_{0.12}$ Ga $_{0.88}$ As/Al $_{0.90}$ Ga $_{0.10}$ As (silicon-doped,  $1.5\times10^{18}$  cm $^{-3}$ ) serving as the bottom DBR mirror. The active region consists of five In $_{0.10}$ Ga $_{0.90}$ As quantum wells, which are confined by Al $_{0.37}$ Ga $_{0.63}$ As barriers. The top DBR mirror consists of 20 pairs of p-type Al $_{0.15}$ Ga $_{0.85}$ As/Al $_{0.90}$ Ga $_{0.10}$ As (carbon doped,  $3\times10^{18}$  cm $^{-3}$ ) capped with a highly conductive p-type GaAs layer (carbon doped,

 $2 \times 10^{19} \,\mathrm{cm}^{-3}$ ). A single 25-nm thick Al<sub>0.98</sub>Ga<sub>0.02</sub>As layer is inserted right above the active region for selective oxidation. The fabrication process begins with the tensilely strained PECVD SiN<sub>x</sub> diffusion mask being deposited and photolithographically patterned. The strained diffusion mask is designed to reduce the lateral diffusion under the diffusion mask while preserving the mask integrity at the disordering temperatures (650 °C). The tensilely-strained PECVD SiN<sub>x</sub> diffusion mask is deposited with 20 sccm SiH<sub>4</sub>, 45 sccm NH<sub>3</sub>, 1960 sccm N<sub>2</sub>, 950 mT pressure, and 40 W of plasma power using a 13.56 MHz RF plasma source at 380 °C table temperature. Using a Bruker Dektak XT DXT-A stylus profilometer, the curvatures of 100 mm silicon calibration wafers are measured before and after the deposition of the films. Through invoking Stoney's equation, the film stress of the tensilestrained  $SiN_x$  film is calculated to be approximately  $+639 \, MPa$ . The diffusion masks are patterned to diameters of 4.0, 4.6, 5.0, 5.1, and  $5.7 \mu m$  corresponding to oxide aperture designs of 9, 10, 11, 12, and 13  $\mu$ m, respectively. The correlation between the optical transversemodes supported by a given oxide-aperture size and the corresponding disorder-defined aperture size that is optimized for single-mode performance utilized here is described in previous work.<sup>20</sup> The masked VCSELs are then sealed under vacuum ( $<5 \times 10^{-6}$  Torr) in a quartz ampoule along with high-purity solid zinc arsenide pieces. The vacuum-sealed quartz ampoule is placed into an annealing furnace at 650 °C for 20 min to diffuse zinc and induce disordering. Afterward, the strained diffusion masks are removed using SF<sub>6</sub> dry etching, and a standard oxide-confined VCSEL fabrication process is carried out. In this process, VCSEL mesas are first defined using chlorine-based ICP-RIE etching with diameters of 25–29  $\mu$ m. *In situ* laser interferometry is used to monitor and precisely terminate the etch after the active region is isolated. The devices are then selectively oxidized at 430 °C to form oxide apertures ranging from 9 to 13  $\mu$ m. The n-type contact (Au/Ge/ Ni/Au) is defined via e-beam evaporation and a liftoff photolithography process and annealed at 380 °C in a N2 ambient to form Ohmic contacts. The devices are then planarized with benzocylobutene (Dow Cyclotene 3022-46) in a vacuum oven at 250 °C. A freon-based RIE etchback process is performed to expose the top of the mesas followed by a patterned via etch to expose the n-contact. The p-contact (Ti/Pt/ Au) is deposited followed by the deposition of an interconnect metal layer (Ti/Au) to form sizable probing pads for characterization. A cross-sectional illustration of the fabricated device is shown in Fig. 1(a). A magnified view of the disorder-defined aperture is shown in Fig. 1(b), where the impurity-induced disordering depth is measured to be approximately 0.8 µm with limited lateral disordering from the tensile-strained diffusion mask. A focused ion beam scanning electron microscopy (FIB-SEM) cross section of the 27  $\mu$ m aperture single-mode IID VCSEL device demonstrated in this work can be seen in Fig. 1(c). It is noted that top p-DBR layers of the device are sufficiently disordered, such that the aluminum composition is too low to facilitate any appreciable oxidation. In the first few p-DBR layers that exhibit lateral oxidation, these layers are only partially disordered, which results in slightly lowered aluminum composition of the high aluminum content p-DBR layers. As the oxidation rate exponentially decreases with aluminum composition, the visual effect of a sloped tapering in these oxide layers is observed. In addition, the oxide layers present in the n-DBR are due to partial etching past the active region during the mesa etch process and are not expected to impact device performance.

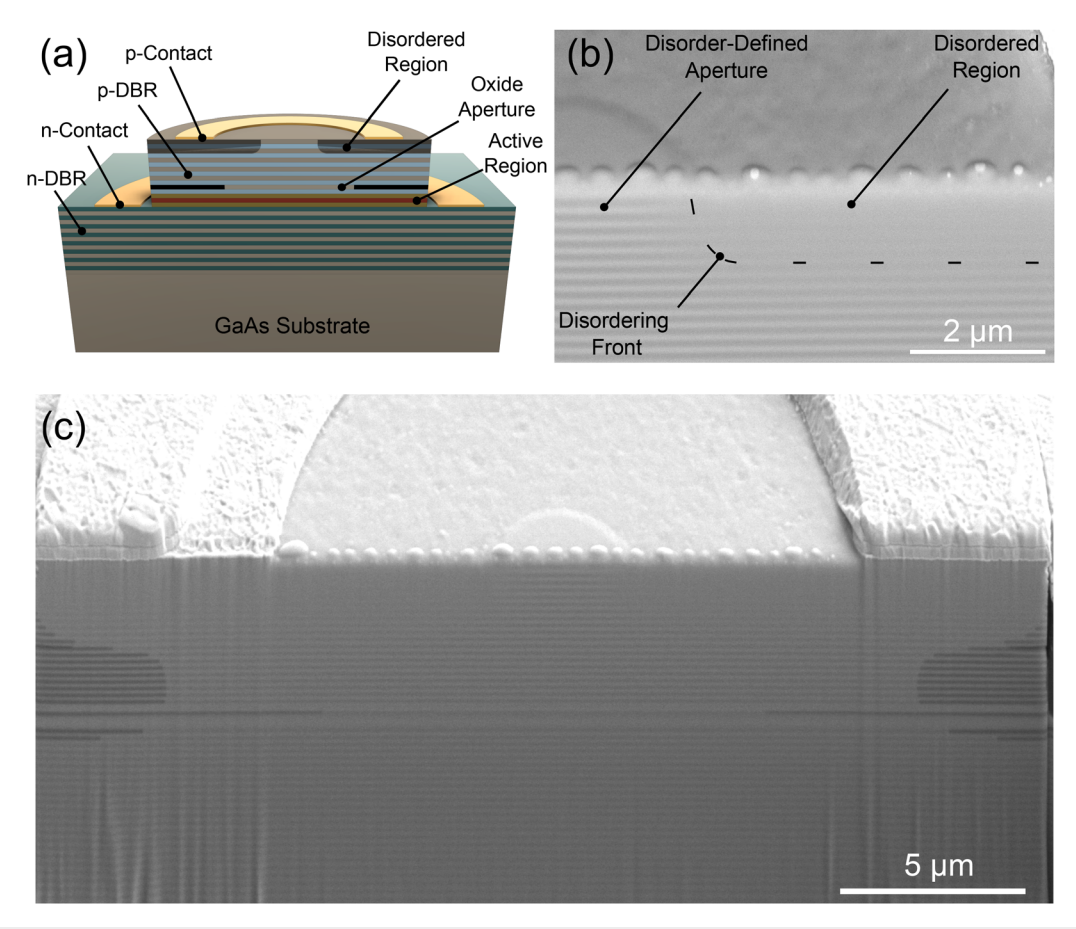
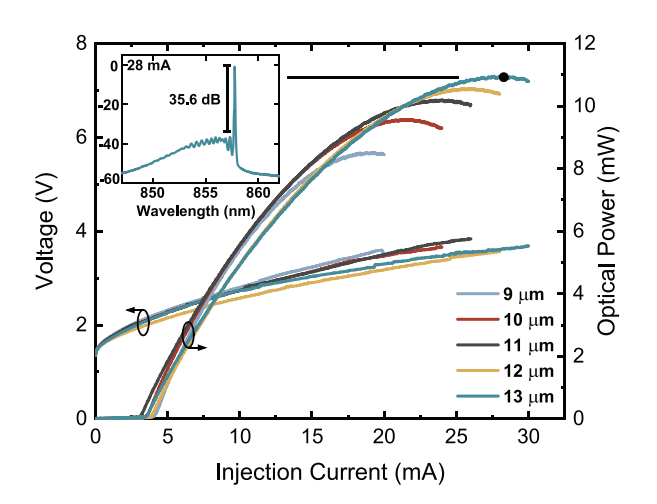


FIG. 1. (a) FIB-SEM of the fabricated disorder-defined VCSEL device. (b) Expanded view of disorder-defined aperture. (c) Cross-sectional schematic of disorder-defined VCSEL fabricated in this work.

The electro-optical performance of the IID VCSELs is characterized through light-current-voltage (L-I-V) measurements, whereas the single mode operating range of the devices is determined through measurements of the optical spectrum. Single-mode operation is defined by a side-mode suppression ratio greater than 30 dB in alignment with other published work. 12,14,20 All measurements taken here are under room-temperature, continuous-wave (CW) operation on unmounted VCSELs via wafer probing. I-V characteristics are measured using an Agilent HP4155C semiconductor parameter analyzer, and the optical output powers (L) are collected using a calibrated (NIST traceable) broad-area silicon photodetector (Newport 818-UV, 200-1100 nm) with an OD3 attenuator to prevent the detector from saturating. Additionally, an anti-reflective coated plano-convex lens (Thorlabs LA1951-AB) is used to collimate the beam for improved light collection efficiency into the detector. For optical spectra measurements, a ball-lensed multimode fiber is used to couple the light into a fiber patch cable that is connected to the multimode input of an HP70951B optical spectrum analyzer with high spectral resolution (0.08 nm) to resolve the modal characteristics. As shown in Fig. 2, the L-I-V of the IID VCSELs ranging from 9 to 13  $\mu$ m in oxide-aperture



**FIG. 2.** I–V (left) and L–I (right) characteristics of the disorder-defined VCSEL devices fabricated and single-mode spectra of the 13  $\mu$ m aperture size device taken at the maximum output power (inset).

size emits record single-mode output powers (8.52, 9.57, 10.20, 10.57, and 10.95 mW, respectively) with SMSRs from the fundamental mode of 34.5, 34.4, 34.3, 33.4, and 35.6 dB, respectively, as shown in Fig. 3. This not only confirms the capabilities of strain-modified disordering apertures in suppressing the higher-order modes of large oxideaperture VCSEL devices, but also verifies significantly enhanced single-mode power. The devices exhibit low differential resistances (92, 82, 79, 64, and 58  $\Omega$ , respectively) that are significantly lower than standard oxide-confined VCSELs with similar aperture sizes  $(>100\,\Omega)$ . The greatly reduced differential series resistance is advantageous for reducing power loss due to Joule heating and for improving impedance matching for high-speed operation. To the authors' knowledge, this is the highest single-fundamental-mode power from any impurity-induced disordered VCSEL reported to date<sup>19</sup> and any monolithic VCSEL design with a similar oxide aperture size.<sup>11</sup> Moreover, these disordered VCSEL devices all exhibit singlefundamental-mode operation throughout their entire operating range. As shown in Fig. 4, the spectral characteristics for the 13  $\mu$ m oxideaperture IID VCSEL device show single-mode operation even up to 30 mA, where thermal rollover begins to occur. As these devices are unmounted and uncooled, the results shown here are expected to be the lower performance limit of these devices. The use of die bonding to a heatsink or temperature-controlled stage is expected to enable even greater single-mode powers. As there were no indications of SMSR reduction from even the largest oxide-aperture size (13  $\mu$ m), this technique is expected to be applicable for larger oxide-aperture devices with the use of appropriately sized disorder-defined apertures. To examine the optical emission profile, near-field imaging is taken for all of the devices using a CMOS image-sensor under 50× magnification. An OD9 filter is placed directly in front of the image sensor to prevent pixels from saturating. The horizontal cut of the near-field beam profile for each device is plotted in Fig. 5, where the near-field pattern from the 13  $\mu$ m oxide-aperture device is shown in the inset. The near-field images were captured at the maximum output power of each device. As shown in Fig. 5, a Gaussian-like optical beam profile is

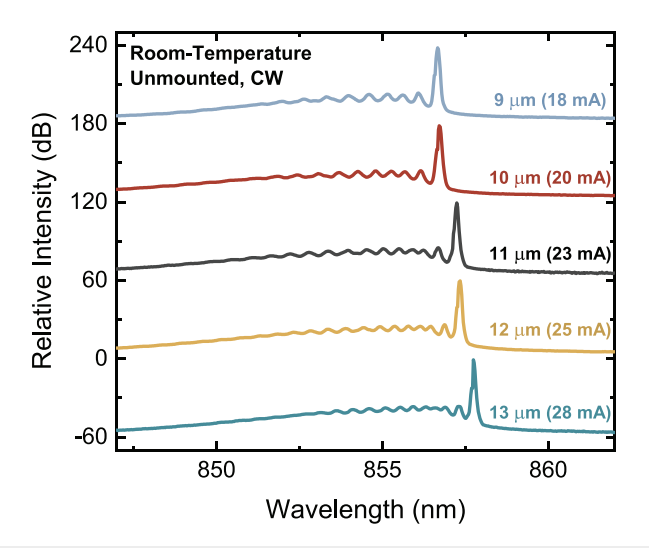


**FIG. 3.** Optical spectra taken at various current injection levels corresponding to the maximum optical output power of the fabricated devices exhibiting single-mode (SMSR > 30 dB) spectra for all devices.

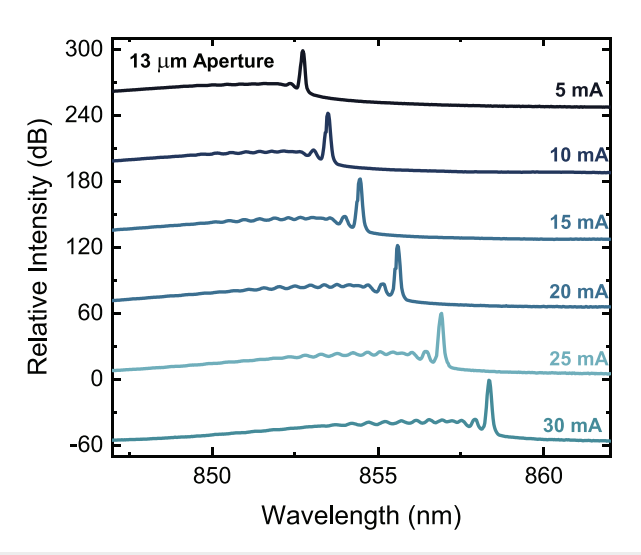


**FIG. 4.** Optical spectra characteristics of the 13  $\mu$ m oxide-aperture for the full current range of the device in 5 mA increments.

observed, verifying single-fundamental-mode operation even at the highest optical output power, which is consistent with the optical spectra shown in Fig. 4.

It is noted that while other work has shown difficulty in suppressing higher-order modes with increasing optical output power and has shown devices even becoming few-moded at their highest optical output powers,  $^{13,14,20}$  the SMSR is seen here to increase with increasing optical output power. The SMSRs of the  $13~\mu m$  oxide-aperture device for current injection levels of  $10{\text -}30~\text{mA}$  in 5 mA steps are 33.3, 34.1, 35.1, 34.6, and 35.5 dB, respectively, showing greater higher-order mode suppression at higher current levels. Possible explanations include thermal lensing where the fundamental mode is focused through the disorder-defined aperture under high current injection;  $^{30}$ 

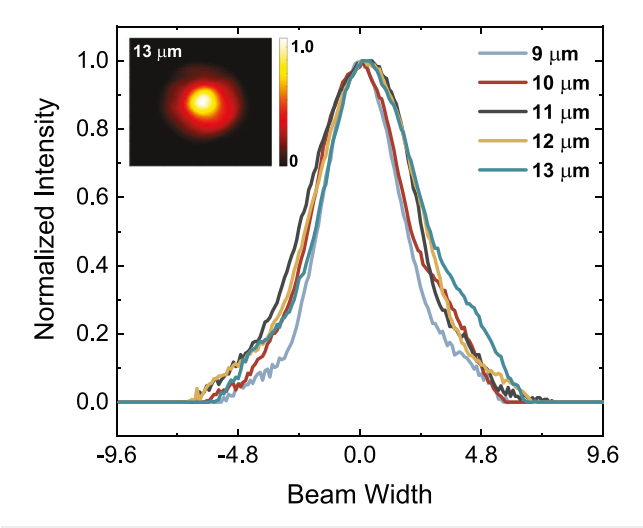


**FIG. 5.** Optical beam width profile from near-field images captured for each IID VCSEL device at the maximum optical output powers.

however, further investigation is needed to confirm the specific reason for the SMSR improvement with power.

In conclusion, the use of strain-controlled disorder-defined apertures in VCSELs is shown to be a promising method for realizing stable high-power single-fundamental-mode operation. The single-mode disorder-defined VCSELs in this work demonstrate single mode output powers greater than 10 mW and show excellent high-order mode suppression throughout their entire operating range. The findings of this work can be applied to other high-performance IID VCSEL designs and can be used to further improve high-speed modulation or beam-shaping characteristics for emerging VCSEL-based systems.

This work was supported in part by the II-VI Foundation and the National Science Foundation under ECCS Grant No. 16-40196 and OAC Grant No. 1827126. This work was carried out in part in the Materials Research Laboratory Central Research Facilities at the University of Illinois at Urbana-Champaign. The authors would also like to thank Professor Nick Holonyak, Jr., for his guidance and insights over the years.

#### **AUTHOR DECLARATIONS**

#### **Conflict of Interest**

The authors have no conflicts to disclose.

# DATA AVAILABILITY

The data that support the findings of this study are available from corresponding author upon reasonable request.

# **REFERENCES**

- <sup>1</sup>M. Dummer, K. Johnson, S. Rothwell, K. Tatah, and M. Hibbs-Brenner, Proc. SPIE 11692, 116920C (2021).
- <sup>2</sup>J. M. Dallesasse, N. Holonyak, Jr., A. R. Sugg, T. A. Richard, and N. El-Zein, Appl. Phys. Lett. 57, 2844 (1990).
- <sup>3</sup>J. M. Dallesasse, N. El-Zein, N. Holonyak, Jr., K. C. Hsieh, R. D. Burnham, and R. D. Dupuis, J. Appl. Phys. 68, 2235 (1990).
- <sup>4</sup>D. L. Huffaker, D. G. Deppe, K. Kumar, and T. J. Rogers, Appl. Phys. Lett. 65, 113087 (1994).
- <sup>5</sup>J. M. Dallesasse and N. Holonyak, Jr., J. Appl. Phys. 113, 051101 (2013).

- <sup>6</sup>C. Jung, R. Jäger, M. Grabherr, P. Schnitzer, R. Michaelzik, B. Weigl, S. Müller, and K. J. Ebeling, Electron. Lett. 33, 1790-1791 (1997).
- <sup>7</sup>D. G. Deppe, M. Li, X. Yang, and M. Bayat, IEEE J. Quantum Electron. 54, 1
- <sup>8</sup>H. Y. Kao, C. T. Tsai, S. F. Leong, C. Y. Peng, Y. C. Chi, H. Y. Wang, H. C. Kuo, C. H. Wu, W. H. Cheng, and G. R. Lin, Photonics. Res 6, 666 (2018).
- <sup>9</sup>C. Y. Huang, H. Y. Wang, C. H. Wu, C. H. Cheng, C. T. Tsai, C. H. Wu, M. Feng, and G. R. Lin, IEEE J. Sel. Top. Quantum. Electron. 26, 1500210 (2020).
- 10 A. Haglund, J. S. Gustavsson, J. Vukusic, P. Modh, and A. Larsson, IEEE Photonics Technol. Lett. 16, 368 (2004).
- <sup>11</sup>A. Furukawa, S. Sasaki, M. Hoshi, A. Matsuzono, K. Moritoh, and T. Baba, Appl. Phys. Lett. 85, 5161 (2004).
- <sup>12</sup>M. C. Huang, Y. Zhou, and C. J. Chang-Hasnain, Appl. Phys. Lett. **92**, 171108
- <sup>13</sup>D. Zhou and L. J. Mawst, IEEE J. Quantum Electron. 38, 1599 (2002).
- <sup>14</sup>B. Kesler, T. O'Brien, G. L. Su, and J. M. Dallesasse, IEEE Photonics Technol. Lett. 28, 1497 (2016).
- <sup>15</sup>W. D. Laidig, N. Holonyak, Jr., M. D. Camras, K. Hess, J. J. Coleman, P. D. Dapkus, and J. Bardeen, Appl. Phys. Lett. **38**, 776 (1981).

  16 N. Holonyak, Jr., IEEE J. Sel. Top. Quantum Electron. **4**, 584 (1998).
- <sup>17</sup>D. G. Deppe and N. Holonyak, Jr., J. Appl. Phys. **64**, R93 (1988).
- <sup>18</sup>P. D. Floyd, M. G. Peters, L. A. Coldren, and J. L. Merz, IEEE Photonics Technol. Lett. 7, 1388 (1995).
- <sup>19</sup>J. W. Shi, Z. R. Wei, L. K. Chi, J. W. Jiang, J. M. Wun, I. C. Lu, J. Chen, and Y. J. Yang, J. Lightwave Technol. 31, 4037 (2013).
- 20T. O'Brien, B. Kesler, S. Al Mulla, and J. M. Dallesasse, IEEE Photonics Technol. Lett. 29, 1179 (2017).
- <sup>21</sup>P. Su, K. P. Pikul, F. C. Hsiao, T. O'Brien, and J. M. Dallesasse, Proc. SPIE 11300, 113000B (2020).
- <sup>22</sup>C. Y. Peng, H. T. Cheng, H. C. Kuo, and C. H. Wu, IEEE Trans. Electron Devices 67, 1041 (2020).
- <sup>23</sup>C. C. Chen, S. J. Liaw, and Y. J. Yang, IEEE Photonics Technol. Lett. 13, 266 (2001).
- <sup>24</sup>P. Su, F. C. Hsiao, T. O'Brien, and J. M. Dallesasse, IEEE Trans. Semicond. Manuf. 31, 447 (2018).
- <sup>25</sup>R. G. Dandrea and C. B. Duke, *Phys. Rev. B* **45**, 14065 (1992).
- <sup>26</sup>S. S. Iyer and F. K. Legoues, J. Appl. Phys. **65**, 4693 (1989).
- 27S. M. Prokes and K. L. Wang, Appl. Phys. Lett. 56, 2628 (1990).
- <sup>28</sup>Y. S. Lim and J. Y. Lee, Appl. Phys. Lett. **80**, 2481 (2002).
- <sup>29</sup>M. H. MacDougal, J. Geske, C. K. Lin, A. E. Bond, and P. D. Dapkus, IEEE Photonics Technol. Lett. 10, 9 (1998).
- 30 R. Amatya, D. Luerssen, M. Farzaneh, and J. A. Hudgings, in CLEO, OSA Technical Digest (OSA Publishing, 2006), p. 1.